

## Appendix A from T. Yamanaka et al., “Generation Separation in Simple Structured Life Cycles: Models and 48 Years of Field Data on a Tea Tortrix Moth”

(Am. Nat., vol. 179, no. 1, p. 95)

### Temperature-Dependent Birth, Death, and Development Rate Functions

As with most insects, the birth rate and stage-specific death and development rates of *Adoxophyes honmai* are strongly temperature dependent. We parameterize this temperature dependence by using data from laboratory experiments of Nabeta et al. (2005) and from insects in the Miyazaki Prefecture (Kodomari et al. 2003). Data include observations of birth rate and development time for eggs, larvae, and pupae, as well as survivorship for all stages at a range of temperatures. The pattern of adult survivorship (see fig. 1 of Nabeta et al. 2005) suggests that adults divide into two substages based on age. The first contains young adults, who suffer relatively low mortality, and the second contains older adults, who have much higher mortality rates. The age of transition between the two substages is temperature dependent and correlates closely to the cessation of reproduction. Thus, we subdivide the adult stage into reproductive and senescent stages. Since only nonsenescent adults reproduce and the senescent mortality rate is much higher than the nonsenescent rate, we include only reproductive adults in the model (table 1). The reproductive-stage duration was calculated as the time to 50% survival.

Development rates increase with increasing temperature in all stages (fig. A1). The empirical data suggest a development-rate function of the logistic form,

$$h_i(t) = \frac{\alpha_i}{1 + \exp(-\gamma_D(D(t) - h_D))}, \quad (\text{A1})$$

where  $D(t)$  is the temperature (degrees Celsius) at time  $t$ ,  $h_D$  is the temperature at which the development-rate function reaches half the asymptotic value,  $\alpha_i$  is a scaling coefficient, and  $\gamma_D$  controls the steepness of the logistic function. We first estimate the parameters  $\alpha$ ,  $h_D$ , and  $\gamma_D$ , which are common to all stages, by fitting equation (A1) to total duration from egg to pupa, using a minimum least squares objective. Using the common  $h_D$  and  $\gamma_D$ , the  $\alpha_i$  for each stage was first estimated in equation (A1) and subsequently estimated by fitting the stage-specific development rates using the same minimum least squares objective. The two larval stages are split at the midpoint of the larval development period ( $\alpha_{L_1}$ ), and both larval sizes are assumed to have the same development rate, which is double that of the full larval stage to ensure that cohorts transition through the two substages at the time for the full stage (i.e.,  $\alpha_{L_1} = \alpha_{L_2} = 2\alpha_{L_1}$ ).

Stage-specific mortality data are available in the form of through-stage survivorship at each temperature. We convert these to daily mortality rates ( $d_{\text{obs}}$ ) by using the relationship,  $d_{\text{obs}} = -\log(\sigma_{\text{obs}})/\tau_{\text{obs}}$ , where  $\sigma_{\text{obs}}$  is the observed survivorship and  $\tau_{\text{obs}}$  is the observed mean development time. Daily mortality rates generally increase with temperature (fig. A2). With the aim of simplifying the model, we fit a mortality function, using the same generic base function as for the development rate, namely,  $d_i(t) = n_i g(t)$ , where  $g(t) = 1/(1 + \exp(-\gamma_D(D(t) - h_D)))$  and  $n_i$  is a stage-specific scalar. The mortality data are more variable than the development data, but the mortality-rate function yields a reasonable fit to the data, with the exception of some mismatches in the larval and pupal stages at high temperatures. Using the same base function for mortality as was found for the development rates greatly simplifies analysis of the model (see below) and had little effect on the predicted population dynamics. The per capita birth rates also show an increase with higher temperature (fig. A3). Following the same rationale as for the mortality rate, we assume a functional form that is proportional to the base function  $b(t) = cg(t)$ . Fit parameter values are shown in table 2.

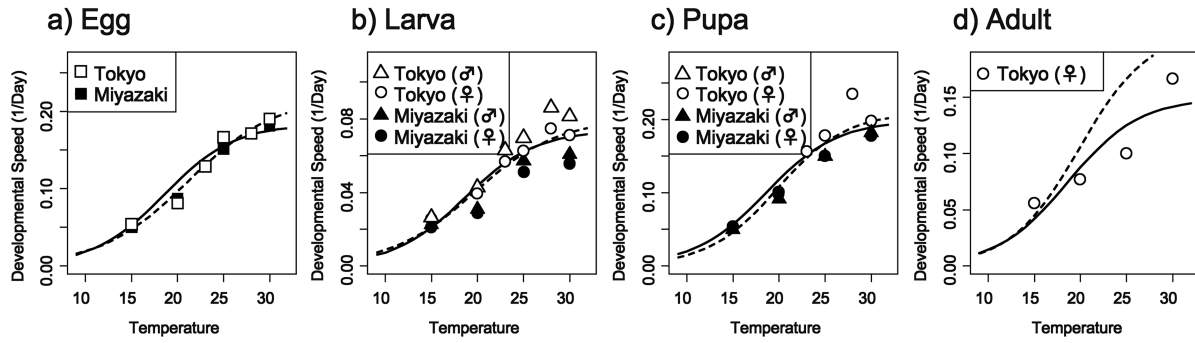


**Figure A1:** Stage-specific development rate ( $h_i(t)$ ) of female moths as a function of temperature. Data are from Tokyo (open symbols) and Miyazaki Prefecture (filled symbols) for the egg (a), larval (b), pupal (c), and reproductive (nonsenescent) adult (d) stages. The development-rate function is assumed to share the common scaling parameters  $h_D$  and  $\gamma_D$  for all stages, but the constants of proportionality  $\alpha_i$  are different for each stage. The solid lines show the fit function, and the dashed lines represent the alternative fit function changing not only  $\alpha_i$ , but also  $h_D$  and  $\gamma_D$ . See table 2 for fit parameter values.

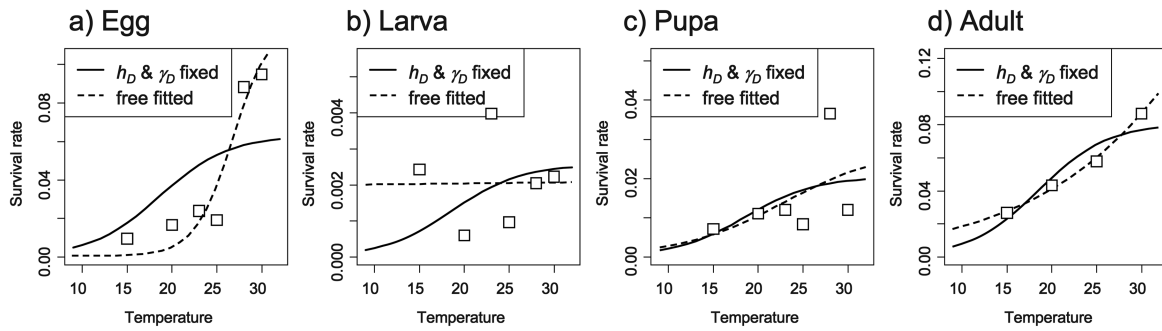


**Figure A2:** Stage-specific mortality rate ( $\delta_i(t)$ ) of female moths as a function of temperature. Data are from Tokyo for the egg (a), larval (b), pupal (c), and reproductive (nonsenescent) adult (d) stages. The mortality-rate function is assumed to have the same base function (i.e.,  $g(t)$ ) as the developmental rate and a constant of proportionality  $n_i$  that is different for each stage. The dashed lines show the function as fitted not only with  $\delta_i$ , but also with  $h_D$  and  $\gamma_D$ . The solid lines show the function with  $h_D$  and  $\gamma_D$  fixed at the estimates from the development-rate data. See table 2 for fit parameter values.

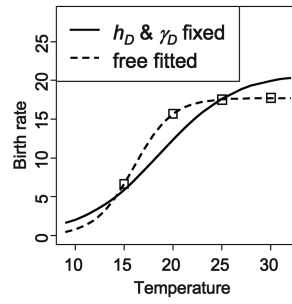


**Figure A3:** Per capita birth rate ( $b(t)$ ) as a function of temperature. Data are from Tokyo. We assume a birth-rate function of the form using the base function with a constant of proportionality  $c$ . The dashed lines show the function as fitted not only with  $\delta_i$  but also with  $h_D$  and  $\gamma_D$ . The solid lines show the function with  $h_D$  and  $\gamma_D$  fixed at the estimates from the development-rate data. See table 2 for fit parameter values.

## **Appendix B from T. Yamanaka et al., “Generation Separation in Simple Structured Life Cycles: Models and 48 Years of Field Data on a Tea Tortrix Moth”**

**(Am. Nat., vol. 179, no. 1, p. 95)**

### **Model Development and Scale Transformation**

#### **Timescale Model**

The modeling framework developed by Nisbet and Gurney (1983) provides a basis for model population dynamics of stage-structured organisms with time-varying birth, death, and development rates (e.g., due to food dynamics or seasonal temperature). In this appendix, we first lay out the overall architecture of the model on a Julian timescale. Subsequently, we transform the equations to a physiologically based scale (hereafter referred to as the phi scale), so that the time-varying delays become fixed delays to facilitate model analysis. The general model was developed to examine the role of density dependence (three types), parasitism, temperature, and adult senescence on population dynamics. Each variant can be arrived at as a special case of the general model.

To incorporate the role of parasitism, the general model requires a description of both moth and parasitoid populations. The tortrix moth population is broken up into five stages: egg (E), young larval ( $L_1$ ), old larval ( $L_2$ ), pupal (P), and adult (A). Wasp populations are assumed to be structured into egg, larval, pupal, and adult stages. However, since the egg, larval, and pupal stages follow the same development as *Adoxophyes honmai* (Takagi 1974; Yukinari 1976), it is necessary only to explicitly track the adult wasps (W) and parasitized *A. honmai* stages (denoted by a superscript W).

In our study, we consider the egg parasitoid *Ascogaster reticulata* (Braconidae). A female wasp oviposits on an egg of the host, *A. honmai*. A larval wasp gets into its host egg and grows inside the host body. At the end of the old-larval stage, it escapes from the host tissue to pupate. For the detailed biology of *A. reticulata*, see Kainoh and Tamaki (1982).

The model architecture is

$$\begin{aligned}
 \frac{dE(t)}{dt} &= R_b(t) - R_E(t) - (d_E(t) + p_w(t))E(t), \\
 \frac{dL_1(t)}{dt} &= R_E(t) - R_{L_1}(t) - d_{L_1}(t)L_1(t), \\
 \frac{dL_2(t)}{dt} &= R_{L_1}(t) - R_{L_2}(t) - d_{L_2}(t)L_2(t), \\
 \frac{dP(t)}{dt} &= R_{L_2}(t) - R_P(t) - d_P(t)P(t), \\
 \frac{dA(t)}{dt} &= R_P(t) - R_A(t) - d_A(t)A(t), \\
 \frac{dL_1^W(t)}{dt} &= p_w(t)E(t) - R_{L_1^W}(t) - d_{L_1^W}(t)L_1^W(t), \\
 \frac{dL_2^W(t)}{dt} &= R_{L_1^W}(t) - R_{L_2^W}(t) - d_{L_2^W}(t)L_2^W(t), \\
 \frac{dP^W(t)}{dt} &= R_{L_2^W}(t) - R_{P^W}(t) - d_{P^W}(t)P^W(t), \\
 \frac{dW(t)}{dt} &= R_{P^W}(t) - d_W(t)W(t),
 \end{aligned} \tag{B1}$$

where  $t$  signifies time-varying functions or states on a Julian-day scale,  $d_i(t)$  is the per capita mortality rate for stage  $i$ , and  $R_i(t)$  is the recruitment out of stage  $i$ , where  $i$  can be the unparasitized moths ( $i \in E, L_1, L_2, P, A$ ), parasitized moths ( $i \in L_1^W, L_2^W, P^W$ ), or adult wasps ( $i \in W$ ). Parasitism occurs through the per capita parasitism rate  $p_w(t)$ , and  $R_b(t)$  represents recruitment into the egg stage from adult reproduction. Note that  $R_A(t)$  represents adult senescence. Since a constant sex ratio is assumed here, only the dynamics of female moths are modeled.

Following Nisbet and Gurney (1983), the recruitment rate into the egg stage is given by

$$R_b(t) = b(t)A(t), \tag{B2}$$

where  $b(t)$  is the per capita birth rate, and recruitment into all other stages is

$$R_{i+1}(t) = R_i(t - \tau_i(t))S_i(t) \frac{h_i(t)}{h_i(t - \tau_i(t))}, \tag{B3}$$

where  $\tau_i(t)$  is the duration of stage  $i$  at time  $t$ ,  $h_i(t)$  is the development rate, and  $S_i(t)$  is the through-stage survivorship. Through-stage survivorship is calculated as

$$S_i(t) = \exp\left(-\int_{t-\tau_i(t)}^t d_i(x)dx\right), \tag{B4}$$

and stage durations are calculated implicitly, using the development-rate constraint

$$1 = \int_{t-\tau_i(t)}^t h_i(x)dx. \tag{B5}$$

Equation (B5) can be used (implicitly) to determine the range in time from  $t - \tau_i(t)$  to  $t$  required for a cohort to

complete stage  $i$ . In numerical simulations, however,  $\tau_i(t)$  is calculated by differentiating both sides for equation (B5) and solving the resulting delay-differential equation (Nisbet and Gurney 1983)

$$\frac{d\tau(t)}{dt} = 1 - \frac{h_i(t)}{h_i(t - \tau_i(t))}. \quad (\text{B6})$$

The set of delay-differential equations given by equation (B1) is the general form of the model on a Julian-day scale. Each model variant is arrived at by specifying a set of birth- ( $b(t)$ ), death- ( $d_i(t)$ ), and development- ( $h_i(t)$ ) rate functions, along with the corresponding parameters. Since the development rate is temperature dependent in this system and temperature varies through time, stage durations will vary through time as well. These time-varying delays can be determined through an integral constraint (eq. [B6]), but this limits the range of mathematical tools available for analysis. Following the approach of McCauley et al. (2008), we transform the model to a physiological scale that results in fixed rather than variable stage durations (except in the specific models of stage-specific winter mortality rates).

### Physiological (Phi)-Scale Model

When the development and mortality rates for all stages are proportional to a single time-varying factor (as laboratory data generally suggest), a transformation to the cumulative development scale results in a model with fixed rather than variable delays (McCauley et al. 2008). In our model, the development rate of the moth scales with temperature as

$$h_i(t) = \frac{\alpha_i}{1 + \exp(-\gamma_D(D(t) - h_D))}, \quad (\text{B7})$$

where  $D(t)$  is the temperature at time  $t$  (see app. A for full details). The stages differ only in their scaling coefficient  $\alpha_i$ . With equation (B7), the expressions used to calculate the stage durations (eq. [B5]) can be rewritten as

$$\frac{1}{\alpha_i} = \int_{t-\tau_i(t)}^t g(x)dx, \quad (\text{B8})$$

where  $g(t) = 1/(1 + \exp(-\gamma_D(D(t) - h_D)))$ . The transformation begins by defining the new physiological scale (phi scale) as

$$\phi(t) = \int_0^t g(x)dx. \quad (\text{B9})$$

For notational clarity, we define  $m(\phi) = g(t)$  as the development rate on the phi scale. From equation (B9), we can write

$$\phi(t - \tau_i(t)) = \int_0^{t-\tau_i(t)} g(x)dx = \int_0^t g(x)dx - \int_{t-\tau_i(t)}^t g(x)dx = \phi(t) - \frac{1}{\alpha_i}, \quad (\text{B10})$$

which reduces the time-varying delay to a fixed delay on the transformed scale. Survivorship equations are also transformed to the phi scale by introducing  $g(x)/g(x)$ ,

$$S_i(t) = \exp\left(-\int_{t-\tau_i(t)}^t d_i(x)dx\right) = \exp\left(-\int_{t-\tau_i(t)}^t \frac{d_i(x)}{g(x)}g(x)dx\right). \quad (\text{B11})$$

From equation (B9), the term  $g(x)dx$  is  $d\phi$ , which lets us write

$$S_i(\phi) = \exp\left(-\int_{\phi-(1/\alpha_i)}^{\phi} \frac{\delta_i(\xi)}{m(\xi)} d\xi\right), \quad (\text{B12})$$

where  $\delta_i(\phi) = d_i(t)$  is the per capita mortality-rate function on the phi scale. To complete the transformation, we take the derivative of equation (B9) with respect to time, which yields

$$\frac{dt}{d\phi} = \frac{1}{m(\phi)}. \quad (\text{B13})$$

Defining  $\beta(\phi) = b(t)$  as the birth-rate function on the phi scale, equation (B2) is rewritten as

$$R_b(\phi) = \beta(\phi)A(\phi), \quad (\text{B14})$$

and the recruitment rates in equation (B3) are

$$R_{i+1}(\phi) = R_i\left(\phi - \frac{1}{\alpha_i}\right)S_i(\phi) \frac{m(\phi)}{m(\phi - (1/\alpha_i))}. \quad (\text{B15})$$

To simplify notation, we introduce cohort-based functions for the delay and survivorship,

$$\phi_i = \phi - \sum_{x=E}^i \frac{1}{\alpha_x}, \quad (\text{B16})$$

$$S_i(\phi) = \exp\left(-\sum_{x=E}^i \int_{\phi_x}^{\phi_{x-1}} \frac{\delta_x(\xi)}{m(\xi)} d\xi\right), \quad (\text{B17})$$

where  $\phi_{E-1} \equiv \phi$  and  $\phi_i$  is the fixed stage duration from the beginning of the egg stage to the end of stage  $i$  ( $i \in \{E, L_1, L_2, P, A\}$ ). Here,  $S_i(\phi)$  is through-stage survivorship from the beginning of the egg stage born at delayed physiological time ( $\phi_i$ ) to stage  $i$  at current physiological time ( $\phi$ ). Using equation (B13) and substituting the above cohort-based expressions, the transformed model equations are given by equation (3).

### Literature Cited Only in the Online Appendixes

Kodomari, S., A. Tataru, Y. Kosugi, and T. Nishijima. 2003. Visual guide of the tea pests and pathogens: new series. Chamber of Tea Association of Shizuoka Prefecture, Shizuoka. (In Japanese.)

**Appendix C from T. Yamanaka et al., "Generation separation in simple structured life-cycles: models and 48 years of field data on a tea tortrix moth"**

**Model variants**

Each model variant is arrived at as a special case of the general model shown in the methods (eq. (3)). The biological mechanisms contained in each model variant (table 3) were chosen to explore various combinations of these processes, always ensuring that models included at least one negatively density dependent mechanism. The following sections detail the simplified model obtained after substituting the functions (table 1) that correspond to each biological mechanisms (see Methods for details).

**Model A: Symmetric larval density-dependence**

$$\begin{aligned} \frac{dL_1(\phi)}{d\phi} &= cA(\phi_E)S_E(\phi) - cA(\phi_{L_1})S_{L_1}(\phi) - (n_L + n_C L(\phi)) L_1(\phi) \\ \frac{dL_2(\phi)}{d\phi} &= cA(\phi_{L_1})S_{L_1}(\phi) - cA(\phi_{L_2})S_{L_2}(\phi) - (n_L + n_C L(\phi)) L_2(\phi) \\ \frac{dA(\phi)}{d\phi} &= cA(\phi_P)S_P(\phi) - n_A A(\phi) \\ S_{L_1}(\phi) &= \exp\left(-\sum_{i=E}^{L_1} \frac{n_i}{\alpha_i} - n_C \int_{\hat{\phi}_{L_1:L_1}}^{\phi} L(\xi) d\xi\right) \\ S_{L_2}(\phi) &= \exp\left(-\sum_{i=E}^{L_2} \frac{n_i}{\alpha_i} - n_C \int_{\hat{\phi}_{L_1:L_2}}^{\phi} L(\xi) d\xi\right) \\ S_P(\phi) &= \exp\left(-\sum_{i=E}^P \frac{n_i}{\alpha_i} - n_C \int_{\hat{\phi}_{L_1:P}}^{\hat{\phi}_{P:P}} L(\xi) d\xi\right) \end{aligned}$$

where  $L(\phi) = L_1(\phi) + L_2(\phi)$ .  $\phi_i$  and  $\hat{\phi}_{j:k}$  were defined as follows and will be used in the subsequent descriptions of model variants.

$$\phi_i = \phi - \sum_{x=E}^i \frac{1}{\alpha_x}$$

$$\hat{\phi}_{j:k} = \begin{cases} \phi - \sum_{x=j}^k \frac{1}{\alpha_x} & \text{if } j \leq k \\ \phi & \text{if } j > k \end{cases}$$

Figure C1 shows the predicted dynamics as a function of the birth rate scalar and adult mortality.

### Model B: Symmetric larval density-dependence with senescence

$$\frac{dL_1(\phi)}{d\phi} = cA(\phi_E)S_E(\phi) - cA(\phi_{L_1})S_{L_1}(\phi) - (n_L + n_C L(\phi)) L_1(\phi)$$

$$\frac{dL_2(\phi)}{d\phi} = cA(\phi_{L_1})S_{L_1}(\phi) - cA(\phi_{L_2})S_{L_2}(\phi) - (n_L + n_C L(\phi)) L_2(\phi)$$

$$\frac{dA(\phi)}{d\phi} = cA(\phi_P)S_P(\phi) - cA(\phi_A)S_A(\phi) - n_A A(\phi)$$

$$S_{L_1}(\phi) = \exp\left(-\sum_{i=E}^{L_1} \frac{n_i}{\alpha_i} - n_C \int_{\hat{\phi}_{L_1:L_1}}^{\phi} L(\xi) d\xi\right)$$

$$S_{L_2}(\phi) = \exp\left(-\sum_{i=E}^{L_2} \frac{n_i}{\alpha_i} - n_C \int_{\hat{\phi}_{L_1:L_2}}^{\phi} L(\xi) d\xi\right)$$

$$S_P(\phi) = \exp\left(-\sum_{i=E}^P \frac{n_i}{\alpha_i} - n_C \int_{\hat{\phi}_{L_1:P}}^{\hat{\phi}_{P:P}} L(\xi) d\xi\right)$$

$$S_A(\phi) = \exp\left(-\sum_{i=E}^A \frac{n_i}{\alpha_i} - n_C \int_{\hat{\phi}_{L_1:A}}^{\hat{\phi}_{P:A}} L(\xi) d\xi\right)$$

where  $L(\phi) = L_1(\phi) + L_2(\phi)$ . Figure C2 shows the predicted dynamics as a function of the birth rate scalar.

**Model C: Symmetric larval density-dependence with Allee effect**

$$\begin{aligned} \frac{dL_1(\phi)}{d\phi} &= c(1 - e^{\nu A(\phi_E)}) A(\phi_E) S_E(\phi) - c(1 - e^{\nu A(\phi_{L_1})}) A(\phi_{L_1}) S_{L_1}(\phi) - (n_L + n_C L(\phi)) L_1(\phi) \\ \frac{dL_2(\phi)}{d\phi} &= c(1 - e^{\nu A(\phi_{L_1})}) A(\phi_{L_1}) S_{L_1}(\phi) - c(1 - e^{\nu A(\phi_{L_2})}) A(\phi_{L_2}) S_{L_2}(\phi) - (n_L + n_C L(\phi)) L_2(\phi) \\ \frac{dA(\phi)}{d\phi} &= c(1 - e^{\nu A(\phi_P)}) A(\phi_P) S_P(\phi) - n_A A(\phi) \\ S_{L_1}(\phi) &= \exp\left(-\sum_{i=E}^{L_1} \frac{n_i}{\alpha_i} - n_C \int_{\hat{\phi}_{L_1:L_1}}^{\phi} L(\xi) d\xi\right) \\ S_{L_2}(\phi) &= \exp\left(-\sum_{i=E}^{L_2} \frac{n_i}{\alpha_i} - n_C \int_{\hat{\phi}_{L_1:L_2}}^{\phi} L(\xi) d\xi\right) \\ S_P(\phi) &= \exp\left(-\sum_{i=E}^P \frac{n_i}{\alpha_i} - n_C \int_{\hat{\phi}_{L_1:P}}^{\phi} L(\xi) d\xi\right) \end{aligned}$$

where  $L(\phi) = L_1(\phi) + L_2(\phi)$ . Figure C3 shows the predicted dynamics as a function of the birth rate scalar and strength of Allee effect.

**Model D: Symmetric larval density-dependence with parasitism**

$$\begin{aligned}
\frac{dE(\phi)}{d\phi} &= cA(\phi) - cA(\phi_E)S_E(\phi) - \left( n_E + k \ln \left( 1 - \frac{u}{k}W(\phi) \right) \right) E(\phi) \\
\frac{dL_1(\phi)}{d\phi} &= cA(\phi_E)S_E(\phi) - cA(\phi_{L_1})S_{L_1}(\phi) - (n_L + n_C L(\phi)) L_1(\phi) \\
\frac{dL_2(\phi)}{d\phi} &= cA(\phi_{L_1})S_{L_1}(\phi) - cA(\phi_{L_2})S_{L_2}(\phi) - (n_L + n_C L(\phi)) L_2(\phi) \\
\frac{dA(\phi)}{d\phi} &= cA(\phi_P)S_P(\phi) - n_A A(\phi) \\
\frac{dW(\phi)}{d\phi} &= k \ln \left( 1 - \frac{u}{k}W(\phi) \right) E(\phi)S_{PW} - n_W W(\phi) \\
S_E(\phi) &= \exp \left( -\frac{n_E}{\alpha_E} - k \int_{\hat{\phi}_{E:E}}^{\phi} \ln \left( 1 - \frac{u}{k}W(\phi) \right) d\xi \right) \\
S_{L_1}(\phi) &= \exp \left( -\sum_{i=E}^{L_1} \frac{n_i}{\alpha_i} - k \int_{\hat{\phi}_{E:L_1}}^{\hat{\phi}_{L_1:L_1}} \ln \left( 1 - \frac{u}{k}W(\phi) \right) d\xi - n_C \int_{\hat{\phi}_{L_1:L_1}}^{\phi} L(\xi) d\xi \right) \\
S_{L_2}(\phi) &= \exp \left( -\sum_{i=E}^{L_2} \frac{n_i}{\alpha_i} - k \int_{\hat{\phi}_{E:L_2}}^{\hat{\phi}_{L_1:L_2}} \ln \left( 1 - \frac{u}{k}W(\phi) \right) d\xi - n_C \int_{\hat{\phi}_{L_1:L_2}}^{\hat{\phi}_{L_2:L_2}} L(\xi) d\xi \right) \\
S_P(\phi) &= \exp \left( -\sum_{i=E}^P \frac{n_i}{\alpha_i} - k \int_{\hat{\phi}_{E:P}}^{\hat{\phi}_{L_1:P}} \ln \left( 1 - \frac{u}{k}W(\phi) \right) d\xi - n_C \int_{\hat{\phi}_{L_1:P}}^{\hat{\phi}_{L_2:P}} L(\xi) d\xi \right) \\
S_{PW}(\phi) &= \exp \left( -\sum_{i=L_1}^P \frac{n_i}{\alpha_i} - n_C \int_{\hat{\phi}_{L_1:P}}^{\hat{\phi}_{L_2:P}} L(\xi) d\xi \right)
\end{aligned}$$

where  $L(\phi) = L_1(\phi) + L_2(\phi)$ . Figure C4 shows the predicted dynamics as a function of the birth rate scalar, search efficiency and interference among wasps.

**Model E: Asymmetrical larval density-dependence**

$$\begin{aligned} \frac{dL_1(\phi)}{d\phi} &= cA(\phi_E)S_E(\phi) - cA(\phi_{L_1})S_{L_1}(\phi) - (n_L + n_C(L_1(\phi) + \psi L_2(\phi))) L_1(\phi) \\ \frac{dL_2(\phi)}{d\phi} &= cA(\phi_{L_1})S_{L_1}(\phi) - cA(\phi_{L_2})S_{L_2}(\phi) - (n_L + n_C(L_1(\phi)/\psi + L_2(\phi))) L_2(\phi) \\ \frac{dA(\phi)}{d\phi} &= cA(\phi_P)S_P(\phi) - n_A A(\phi) \\ S_{L_1}(\phi) &= \exp\left(-\sum_{i=E}^{L_1} \frac{n_i}{\alpha_i} - n_C \int_{\hat{\phi}_{L_1:L_1}}^{\phi} (L_1(\xi) + \psi L_2(\xi)) d\xi\right) \\ S_{L_2}(\phi) &= \exp\left(-\sum_{i=E}^{L_2} \frac{n_i}{\alpha_i} - n_C \int_{\hat{\phi}_{L_1:L_2}}^{\hat{\phi}_{L_2:L_2}} (L_1(\xi) + \psi L_2(\xi)) d\xi - n_C \int_{\hat{\phi}_{L_2:L_2}}^{\phi} (L_1(\xi)/\psi + L_2(\xi)) d\xi\right) \\ S_P(\phi) &= \exp\left(-\sum_{i=E}^P \frac{n_i}{\alpha_i} - n_C \int_{\hat{\phi}_{L_1:P}}^{\hat{\phi}_{L_2:P}} (L_1(\xi) + \psi L_2(\xi)) d\xi - n_C \int_{\hat{\phi}_{L_2:P}}^{\hat{\phi}_{P:P}} (L_1(\xi)/\psi + L_2(\xi)) d\xi\right) \end{aligned}$$

Figure C5 shows the predicted dynamics as a function of the birth rate scalar and strength of competition asymmetry.

**Model F: Asymmetrical larval density-dependence with senescence**

$$\begin{aligned} \frac{dL_1(\phi)}{d\phi} &= cA(\phi_E)S_E(\phi) - cA(\phi_{L_1})S_{L_1}(\phi) - (n_L + n_C(L_1(\phi) + \psi L_2(\phi))) L_1(\phi) \\ \frac{dL_2(\phi)}{d\phi} &= cA(\phi_{L_1})S_{L_1}(\phi) - cA(\phi_{L_2})S_{L_2}(\phi) - (n_L + n_C(L_1(\phi)/\psi + L_2(\phi))) L_2(\phi) \\ \frac{dA(\phi)}{d\phi} &= cA(\phi_P)S_P(\phi) - cA(\phi_A)S_A(\phi) - n_A A(\phi) \\ S_{L_1}(\phi) &= \exp\left(-\sum_{i=E}^{L_1} \frac{n_i}{\alpha_i} - n_C \int_{\hat{\phi}_{L_1:L_1}}^{\phi} (L_1(\xi) + \psi L_2(\xi)) d\xi\right) \\ S_{L_2}(\phi) &= \exp\left(-\sum_{i=E}^{L_2} \frac{n_i}{\alpha_i} - n_C \int_{\hat{\phi}_{L_1:L_2}}^{\hat{\phi}_{L_2:L_2}} (L_1(\xi) + \psi L_2(\xi)) d\xi - n_C \int_{\hat{\phi}_{L_2:L_2}}^{\phi} (L_1(\xi)/\psi + L_2(\xi)) d\xi\right) \\ S_P(\phi) &= \exp\left(-\sum_{i=E}^P \frac{n_i}{\alpha_i} - n_C \int_{\hat{\phi}_{L_1:P}}^{\hat{\phi}_{L_2:P}} (L_1(\xi) + \psi L_2(\xi)) d\xi - n_C \int_{\hat{\phi}_{L_2:P}}^{\hat{\phi}_{P:P}} (L_1(\xi)/\psi + L_2(\xi)) d\xi\right) \\ S_A(\phi) &= \exp\left(-\sum_{i=E}^A \frac{n_i}{\alpha_i} - n_C \int_{\hat{\phi}_{L_1:A}}^{\hat{\phi}_{L_2:A}} (L_1(\xi) + \psi L_2(\xi)) d\xi - n_C \int_{\hat{\phi}_{L_2:A}}^{\hat{\phi}_{P:A}} (L_1(\xi)/\psi + L_2(\xi)) d\xi\right) \end{aligned}$$

Figure C6 shows the predicted dynamics as a function of the birth rate scalar and strength of competition asymmetry.

**Model G: Asymmetrical larval density-dependence with Allee effect**

$$\begin{aligned}
 \frac{dL_1(\phi)}{d\phi} &= c(1 - e^{\nu A(\phi_E)}) A(\phi_E) S_E(\phi) - c(1 - e^{\nu A(\phi_{L_1})}) A(\phi_{L_1}) S_{L_1}(\phi) \\
 &\quad - (n_L + n_C(L_1(\phi) + \psi L_2(\phi))) L_1(\phi) \\
 \frac{dL_2(\phi)}{d\phi} &= c(1 - e^{\nu A(\phi_{L_1})}) A(\phi_{L_1}) S_{L_1}(\phi) - c(1 - e^{\nu A(\phi_{L_2})}) A(\phi_{L_2}) S_{L_2}(\phi) \\
 &\quad - (n_L + n_C(L_1(\phi)/\psi + L_2(\phi))) L_2(\phi) \\
 \frac{dA(\phi)}{d\phi} &= c(1 - e^{\nu A(\phi_P)}) A(\phi_P) S_P(\phi) - n_A A(\phi) \\
 S_{L_1}(\phi) &= \exp\left(-\sum_{i=E}^{L_1} \frac{n_i}{\alpha_i} - n_C \int_{\hat{\phi}_{L_1:L_1}}^{\phi} (L_1(\xi) + \psi L_2(\xi)) d\xi\right) \\
 S_{L_2}(\phi) &= \exp\left(-\sum_{i=E}^{L_2} \frac{n_i}{\alpha_i} - n_C \int_{\hat{\phi}_{L_1:L_2}}^{\hat{\phi}_{L_2:L_2}} (L_1(\xi) + \psi L_2(\xi)) d\xi - n_C \int_{\hat{\phi}_{L_2:L_2}}^{\phi} (L_1(\xi)/\psi + L_2(\xi)) d\xi\right) \\
 S_P(\phi) &= \exp\left(-\sum_{i=E}^P \frac{n_i}{\alpha_i} - n_C \int_{\hat{\phi}_{L_1:P}}^{\hat{\phi}_{L_2:P}} (L_1(\xi) + \psi L_2(\xi)) d\xi - n_C \int_{\hat{\phi}_{L_2:P}}^{\hat{\phi}_{P:P}} (L_1(\xi)/\psi + L_2(\xi)) d\xi\right)
 \end{aligned}$$

Figure C7 shows the predicted dynamics as a function of the birth rate scalar and strength of competition asymmetry.

**Model H: Asymmetrical larval density-dependence with parasitism**

$$\begin{aligned}\frac{dE(\phi)}{d\phi} &= cA(\phi) - cA(\phi_E)S_E(\phi) - \left(n_E + k \ln \left(1 - \frac{u}{k}W(\phi)\right)\right) E(\phi) \\ \frac{dL_1(\phi)}{d\phi} &= cA(\phi_E)S_E(\phi) - cA(\phi_{L_1})S_{L_1}(\phi) - (n_L + n_C(L_1(\phi) + \psi L_2(\phi))) L_1(\phi) \\ \frac{dL_2(\phi)}{d\phi} &= cA(\phi_{L_1})S_{L_1}(\phi) - cA(\phi_{L_2})S_{L_2}(\phi) - (n_L + n_C(L_1(\phi) + \psi L_2(\phi))) L_2(\phi) \\ \frac{dA(\phi)}{d\phi} &= cA(\phi_P)S_P(\phi) - n_A A(\phi) \\ \frac{dW(\phi)}{d\phi} &= k \ln \left(1 - \frac{u}{k}W(\phi)\right) E(\phi) S_{PW} - n_W W(\phi)\end{aligned}$$

$$\begin{aligned}S_E(\phi) &= \exp \left( -\frac{n_E}{\alpha_E} - k \int_{\hat{\phi}_{E:E}}^{\phi} \ln \left(1 - \frac{u}{k}W(\phi)\right) d\xi \right) \\ S_{L_1}(\phi) &= \exp \left( -\sum_{i=E}^{L_1} \frac{n_i}{\alpha_i} - k \int_{\hat{\phi}_{E:L_1}}^{\hat{\phi}_{L_1:L_1}} \ln \left(1 - \frac{u}{k}W(\phi)\right) d\xi \right. \\ &\quad \left. - n_C \int_{\hat{\phi}_{L_1:L_1}}^{\phi} L_1(\xi) + \psi L_2(\xi) d\xi \right) \\ S_{L_2}(\phi) &= \exp \left( -\sum_{i=E}^{L_2} \frac{n_i}{\alpha_i} - k \int_{\hat{\phi}_{E:L_2}}^{\hat{\phi}_{L_1:L_2}} \ln \left(1 - \frac{u}{k}W(\phi)\right) d\xi - n_C \int_{\hat{\phi}_{L_1:L_2}}^{\hat{\phi}_{L_2:L_2}} L_1(\xi) + \psi L_2(\xi) d\xi \right. \\ &\quad \left. - n_C \int_{\hat{\phi}_{L_2:L_2}}^{\phi} L_1(\xi)/\psi + L_2(\xi) d\xi \right) \\ S_P(\phi) &= \exp \left( -\sum_{i=E}^P \frac{n_i}{\alpha_i} - k \int_{\hat{\phi}_{E:P}}^{\hat{\phi}_{L_1:P}} \ln \left(1 - \frac{u}{k}W(\phi)\right) d\xi - n_C \int_{\hat{\phi}_{L_1:P}}^{\hat{\phi}_{L_2:P}} L_1(\xi) + \psi L_2(\xi) d\xi \right. \\ &\quad \left. - n_C \int_{\hat{\phi}_{L_2:P}}^{\hat{\phi}_{P:P}} L_1(\xi)/\psi + L_2(\xi) d\xi \right) \\ S_{PW}(\phi) &= \exp \left( -\sum_{i=L_1}^P \frac{n_i}{\alpha_i} - n_C \int_{\hat{\phi}_{L_1:P}}^{\hat{\phi}_{L_2:P}} L_1(\xi) + \psi L_2(\xi) d\xi - n_C \int_{\hat{\phi}_{L_2:P}}^{\hat{\phi}_{P:P}} L_1(\xi)/\psi + L_2(\xi) d\xi \right)\end{aligned}$$

Figure C8 shows the predicted dynamics as a function of the birth rate scalar, search efficiency and interference among wasps.

**Model I: Parasitism**

$$\begin{aligned}
 \frac{dE(\phi)}{d\phi} &= cA(\phi) - cA(\phi_E)S_E(\phi) - \left( n_E + k \ln \left( 1 - \frac{u}{k}W(\phi) \right) \right) E(\phi) \\
 \frac{dA(\phi)}{d\phi} &= cA(\phi_P)S_P(\phi) - n_AA(\phi) \\
 \frac{dW(\phi)}{d\phi} &= k \ln \left( 1 - \frac{u}{k}W(\phi) \right) E(\phi_P)S_{PW} - n_WW(\phi) \\
 S_E(\phi) &= \exp \left( -\frac{n_E}{\alpha_E} - k \int_{\hat{\phi}_{E:E}}^{\phi} \ln \left( 1 - \frac{u}{k}W(\phi) \right) d\xi \right) \\
 S_P(\phi) &= \exp \left( -\sum_{i=E}^P \frac{n_i}{\alpha_i} - k \int_{\hat{\phi}_{E:P}}^{\hat{\phi}_{L_1:P}} \ln \left( 1 - \frac{u}{k}W(\phi) \right) d\xi \right) \\
 S_{PW}(\phi) &= \exp \left( -\sum_{i=L_1}^P \frac{n_i}{\alpha_i} \right)
 \end{aligned}$$

Figure C9 shows the predicted dynamics as a function of the birth rate scalar, search efficiency and interference among wasps.

**Model J: Symmetric larval density-dependence with winter mortality**

$$\frac{dE(\phi)}{d\phi} = cA(\phi) - cA(\phi_E)S_E(\phi) - \left( n_E + n_{q_1} \frac{e^{-n_{q_2}m(\phi)}}{m(\phi)} \right) E(\phi)$$

$$\frac{dL_1(\phi)}{d\phi} = cA(\phi_E)S_E(\phi) - cA(\phi_{L_1})S_{L_1}(\phi) - (n_L + n_C L(\phi)) L_1(\phi)$$

$$\frac{dL_2(\phi)}{d\phi} = cA(\phi_{L_1})S_{L_1}(\phi) - cA(\phi_{L_2})S_{L_2}(\phi) - (n_L + n_C L(\phi)) L_2(\phi)$$

$$\frac{dP(\phi)}{d\phi} = cA(\phi_{L_2})S_{L_2}(\phi) - cA(\phi_P)S_P(\phi) - \left( n_P + n_{q_1} \frac{e^{-n_{q_2}m(\phi)}}{m(\phi)} \right) P(\phi)$$

$$\frac{dA(\phi)}{d\phi} = cA(\phi_P)S_P(\phi) - \left( n_A + n_{q_1} \frac{e^{-n_{q_2}m(\phi)}}{m(\phi)} \right) A(\phi)$$

$$S_E(\phi) = \exp \left( -\frac{n_E}{\alpha_E} - n_{q_1} \int_{\hat{\phi}_{E:E}}^{\phi} \frac{e^{-n_{q_2}m(\xi)}}{m(\xi)} d\xi \right)$$

$$S_{L_1}(\phi) = \exp \left( -\sum_{i=E}^{L_1} \frac{n_i}{\alpha_i} - n_{q_1} \int_{\hat{\phi}_{E:L_1}}^{\hat{\phi}_{L_1:L_1}} \frac{e^{-n_{q_2}m(\xi)}}{m(\xi)} d\xi - n_C \int_{\hat{\phi}_{L_1:L_1}}^{\phi} L(\xi) d\xi \right)$$

$$S_{L_2}(\phi) = \exp \left( -\sum_{i=E}^{L_2} \frac{n_i}{\alpha_i} - n_{q_1} \int_{\hat{\phi}_{E:L_2}}^{\hat{\phi}_{L_1:L_2}} \frac{e^{-n_{q_2}m(\xi)}}{m(\xi)} d\xi - n_C \int_{\hat{\phi}_{L_1:L_2}}^{\phi} L(\xi) d\xi \right)$$

$$S_P(\phi) = \exp \left( -\sum_{i=E}^P \frac{n_i}{\alpha_i} - n_{q_1} \int_{\hat{\phi}_{E:P}}^{\hat{\phi}_{L_1:P}} \frac{e^{-n_{q_2}m(\xi)}}{m(\xi)} d\xi - n_C \int_{\hat{\phi}_{L_1:P}}^{\hat{\phi}_{P:P}} L(\xi) d\xi - n_{q_1} \int_{\hat{\phi}_{P:P}}^{\phi} \frac{e^{-n_{q_2}m(\xi)}}{m(\xi)} d\xi \right)$$

where  $L(\phi) = L_1(\phi) + L_2(\phi)$ . Figure C10 shows the predicted dynamics as a function with a realistic temperature driver.

**Model K: Symmetrical larval competition with senescence and winter mortality**

$$\begin{aligned}
\frac{dE(\phi)}{d\phi} &= cA(\phi) - cA(\phi_E)S_E(\phi) - \left( n_E + n_{q_1} \frac{e^{-n_{q_2}m(\phi)}}{m(\phi)} \right) E(\phi) \\
\frac{dL_1(\phi)}{d\phi} &= cA(\phi_E)S_E(\phi) - cA(\phi_{L_1})S_{L_1}(\phi) - (n_L + n_C L(\phi)) L_1(\phi) \\
\frac{dL_2(\phi)}{d\phi} &= cA(\phi_{L_1})S_{L_1}(\phi) - cA(\phi_{L_2})S_{L_2}(\phi) - (n_L + n_C L(\phi)) L_2(\phi) \\
\frac{dP(\phi)}{d\phi} &= cA(\phi_{L_2})S_{L_2}(\phi) - cA(\phi_P)S_P(\phi) - \left( n_P + n_{q_1} \frac{e^{-n_{q_2}m(\phi)}}{m(\phi)} \right) P(\phi) \\
\frac{dA(\phi)}{d\phi} &= cA(\phi_P)S_P(\phi) - cA(\phi_A)S_A(\phi) - \left( n_A + n_{q_1} \frac{e^{-n_{q_2}m(\phi)}}{m(\phi)} \right) A(\phi) \\
S_E(\phi) &= \exp \left( -\frac{n_E}{\alpha_E} - n_{q_1} \int_{\hat{\phi}_{E:E}}^{\phi} \frac{e^{-n_{q_2}m(\xi)}}{m(\xi)} d\xi \right) \\
S_{L_1}(\phi) &= \exp \left( -\sum_{i=E}^{L_1} \frac{n_i}{\alpha_i} - n_{q_1} \int_{\hat{\phi}_{E:L_1}}^{\hat{\phi}_{L_1:L_1}} \frac{e^{-n_{q_2}m(\xi)}}{m(\xi)} d\xi - n_C \int_{\hat{\phi}_{L_1:L_1}}^{\phi} L(\xi) d\xi \right) \\
S_{L_2}(\phi) &= \exp \left( -\sum_{i=E}^{L_2} \frac{n_i}{\alpha_i} - n_{q_1} \int_{\hat{\phi}_{E:L_2}}^{\hat{\phi}_{L_1:L_2}} \frac{e^{-n_{q_2}m(\xi)}}{m(\xi)} d\xi - n_C \int_{\hat{\phi}_{L_1:L_2}}^{\phi} L(\xi) d\xi \right) \\
S_P(\phi) &= \exp \left( -\sum_{i=E}^P \frac{n_i}{\alpha_i} - n_{q_1} \int_{\hat{\phi}_{E:P}}^{\hat{\phi}_{L_1:P}} \frac{e^{-n_{q_2}m(\xi)}}{m(\xi)} d\xi - n_C \int_{\hat{\phi}_{L_1:P}}^{\hat{\phi}_{P:P}} L(\xi) d\xi - n_{q_1} \int_{\hat{\phi}_{P:P}}^{\phi} \frac{e^{-n_{q_2}m(\xi)}}{m(\xi)} d\xi \right) \\
S_A(\phi) &= \exp \left( -\sum_{i=E}^A \frac{n_i}{\alpha_i} - n_{q_1} \int_{\hat{\phi}_{E:A}}^{\hat{\phi}_{L_1:A}} \frac{e^{-n_{q_2}m(\xi)}}{m(\xi)} d\xi - n_C \int_{\hat{\phi}_{L_1:A}}^{\hat{\phi}_{P:A}} L(\xi) d\xi - n_{q_1} \int_{\hat{\phi}_{P:A}}^{\phi} \frac{e^{-n_{q_2}m(\xi)}}{m(\xi)} d\xi \right)
\end{aligned}$$

where  $L(\phi) = L_1(\phi) + L_2(\phi)$ . Figure C11 shows the predicted dynamics as a function with a realistic temperature driver.

**Model L: Symmetrical larval competition with Allee effect and winter mortality**

$$\begin{aligned}
\frac{dE(\phi)}{d\phi} &= c(1 - e^{\nu A(\phi)}) A(\phi) - c(1 - e^{\nu A(\phi_E)}) A(\phi_E) S_E(\phi) - \left( n_E + n_{q_1} \frac{e^{-n_{q_2} m(\phi)}}{m(\phi)} \right) E(\phi) \\
\frac{dL_1(\phi)}{d\phi} &= c(1 - e^{\nu A(\phi_E)}) A(\phi_E) S_E(\phi) - c(1 - e^{\nu A(\phi_{L_1})}) A(\phi_{L_1}) S_{L_1}(\phi) - (n_L + n_C L(\phi)) L_1(\phi) \\
\frac{dL_2(\phi)}{d\phi} &= c(1 - e^{\nu A(\phi_{L_1})}) A(\phi_{L_1}) S_{L_1}(\phi) - c(1 - e^{\nu A(\phi_{L_2})}) A(\phi_{L_2}) S_{L_2}(\phi) - (n_L + n_C L(\phi)) L_2(\phi) \\
\frac{dP(\phi)}{d\phi} &= c(1 - e^{\nu A(\phi_{L_2})}) A(\phi_{L_2}) S_{L_2}(\phi) - c(1 - e^{\nu A(\phi_P)}) A(\phi_P) S_P(\phi) - \left( n_P + n_{q_1} \frac{e^{-n_{q_2} m(\phi)}}{m(\phi)} \right) P(\phi) \\
\frac{dA(\phi)}{d\phi} &= c(1 - e^{\nu A(\phi_P)}) A(\phi_P) S_P(\phi) - \left( n_A + n_{q_1} \frac{e^{-n_{q_2} m(\phi)}}{m(\phi)} \right) A(\phi) \\
S_E(\phi) &= \exp \left( -\frac{n_E}{\alpha_E} - n_{q_1} \int_{\hat{\phi}_{E:E}}^{\phi} \frac{e^{-n_{q_2} m(\xi)}}{m(\xi)} d\xi \right) \\
S_{L_1}(\phi) &= \exp \left( -\sum_{i=E}^{L_1} \frac{n_i}{\alpha_i} - n_{q_1} \int_{\hat{\phi}_{E:L_1}}^{\hat{\phi}_{L_1:L_1}} \frac{e^{-n_{q_2} m(\xi)}}{m(\xi)} d\xi - n_C \int_{\hat{\phi}_{L_1:L_1}}^{\phi} L(\xi) d\xi \right) \\
S_{L_2}(\phi) &= \exp \left( -\sum_{i=E}^{L_2} \frac{n_i}{\alpha_i} - n_{q_1} \int_{\hat{\phi}_{E:L_2}}^{\hat{\phi}_{L_1:L_2}} \frac{e^{-n_{q_2} m(\xi)}}{m(\xi)} d\xi - n_C \int_{\hat{\phi}_{L_1:L_2}}^{\phi} L(\xi) d\xi \right) \\
S_P(\phi) &= \exp \left( -\sum_{i=E}^P \frac{n_i}{\alpha_i} - n_{q_1} \int_{\hat{\phi}_{E:P}}^{\hat{\phi}_{L_1:P}} \frac{e^{-n_{q_2} m(\xi)}}{m(\xi)} d\xi - n_C \int_{\hat{\phi}_{L_1:P}}^{\hat{\phi}_{P:P}} L(\xi) d\xi - n_{q_1} \int_{\hat{\phi}_{P:P}}^{\phi} \frac{e^{-n_{q_2} m(\xi)}}{m(\xi)} d\xi \right)
\end{aligned}$$

where  $L(\phi) = L_1(\phi) + L_2(\phi)$ . Figure C12 shows the predicted dynamics as a function with a realistic temperature driver.

Model A

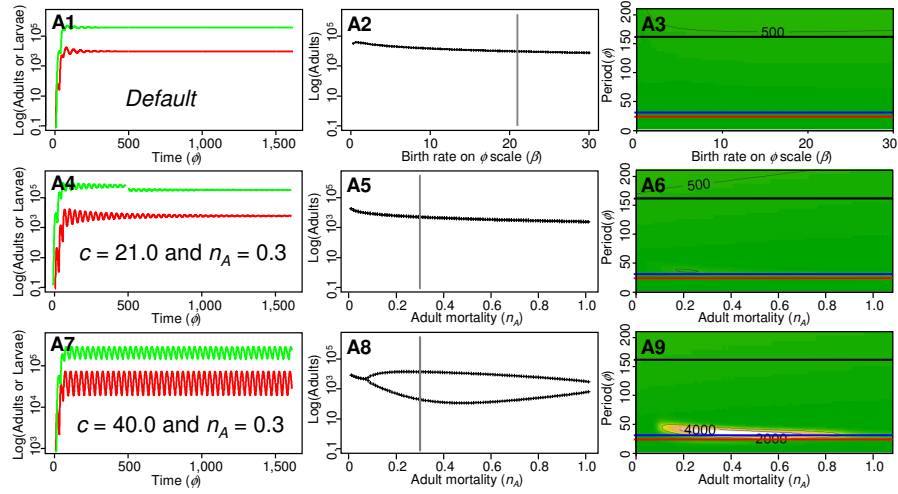


Fig. C1.— Illustrative model dynamics for Model A. Left hand panel shows adult (red) and larval (green) dynamics, middle panel is the bifurcation plot showing the maximum and minimum of adult abundance as a function of a model parameter, and right panel is a color map of the the corresponding periodogram. The vertical gray line in the middle panel indicates parameter location for the simulation in the left panel, and parameters other than those given are in table 2. Horizontal lines on the periodogram are the reference lines from fig. 2. Each row illustrates the change in dynamics as a function of a model parameter.

Model B

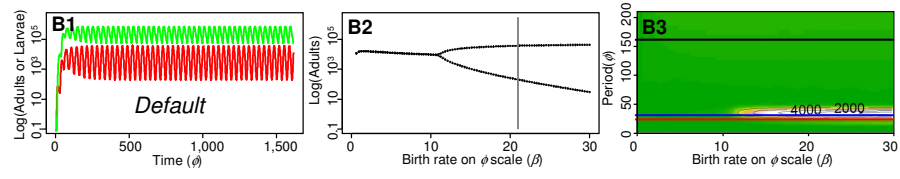


Fig. C2.— Illustrative model dynamics for Model B. See fig. C1 for legend details.

Model C

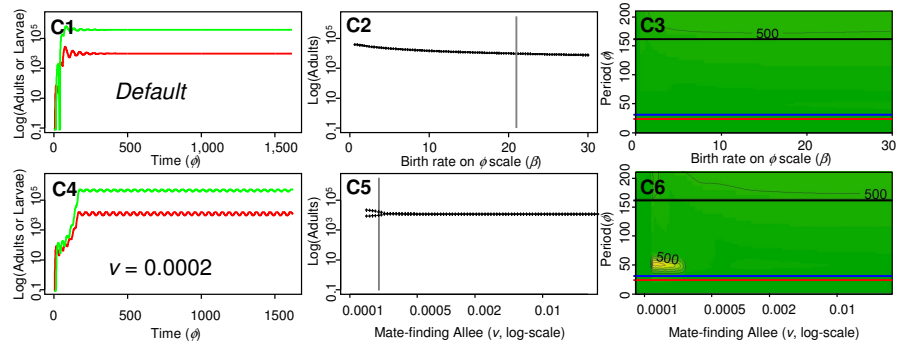


Fig. C3.— Illustrative model dynamics for Model C. See fig. C1 for legend details.

## Model D

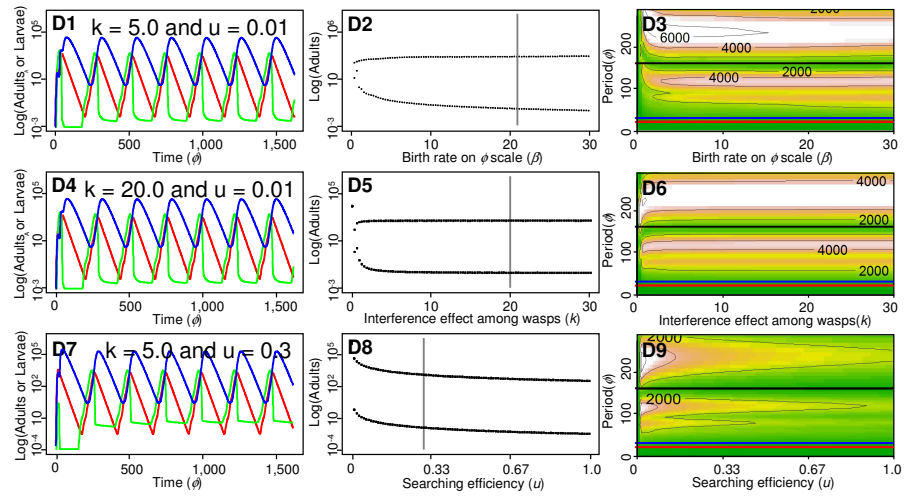


Fig. C4.— Illustrative model dynamics for Model D. See fig. C1 for legend details.

## Model E

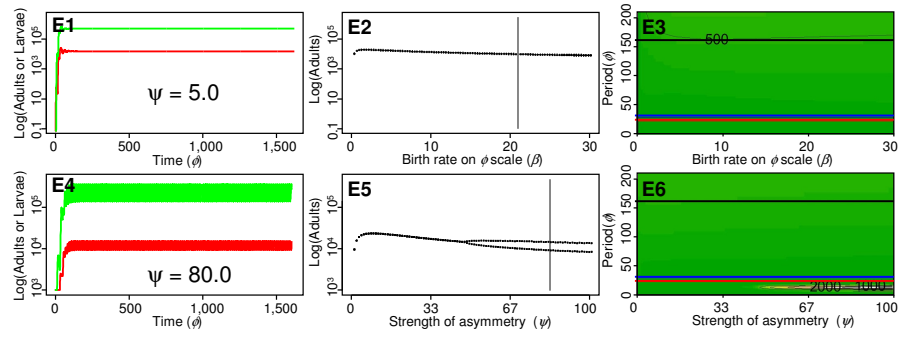


Fig. C5.— Illustrative model dynamics for Model E. See fig. C1 for legend details.

## Model F

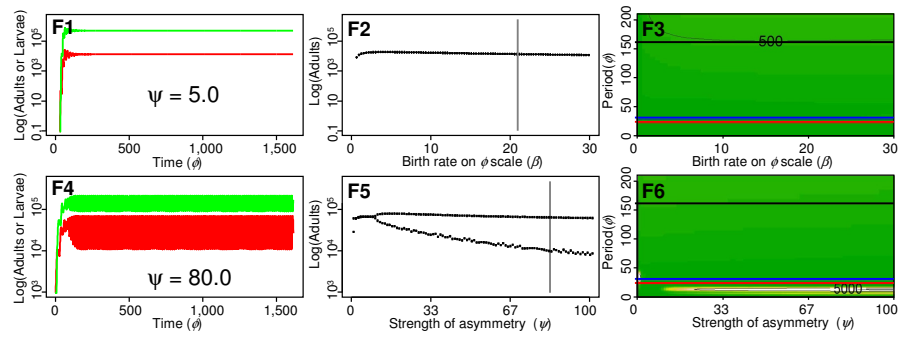


Fig. C6.— Illustrative model dynamics for Model F. See fig. C1 for legend details.

## Model G

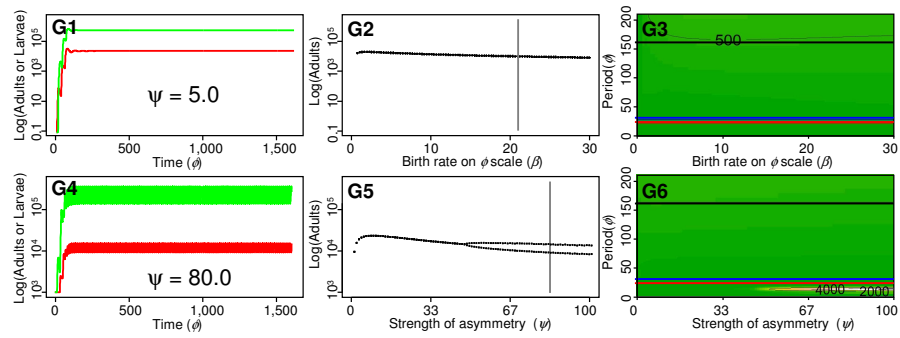


Fig. C7.— Illustrative model dynamics for Model G. See fig. C1 for legend details.

## Model H

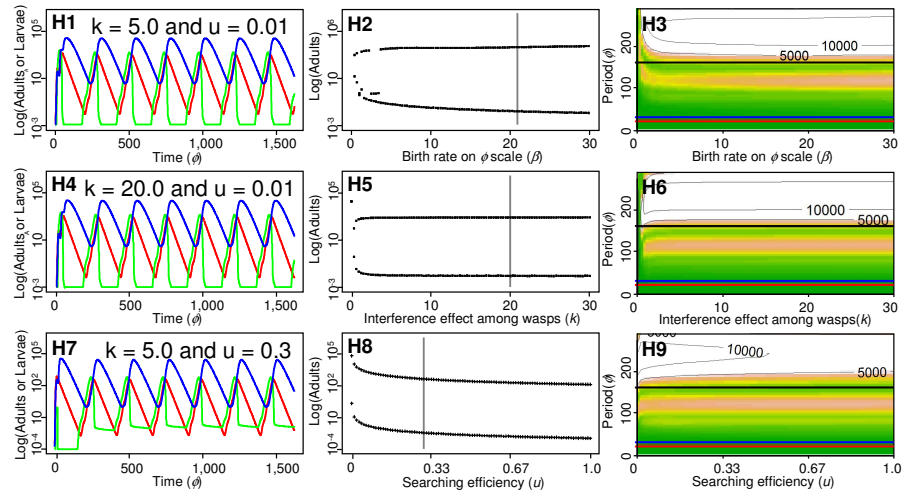


Fig. C8.— Illustrative model dynamics for Model H. See fig. C1 for legend details.

## Model I

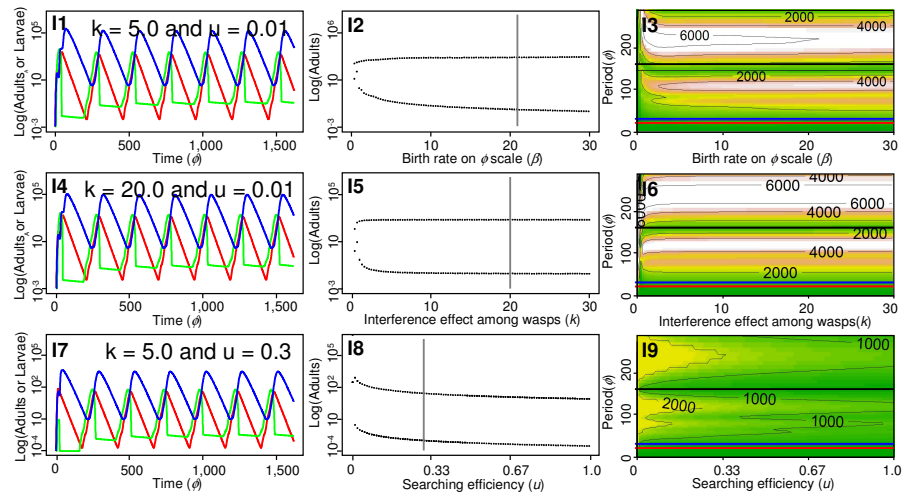


Fig. C9.— Illustrative model dynamics for Model I. See fig. C1 for legend details.

Model J

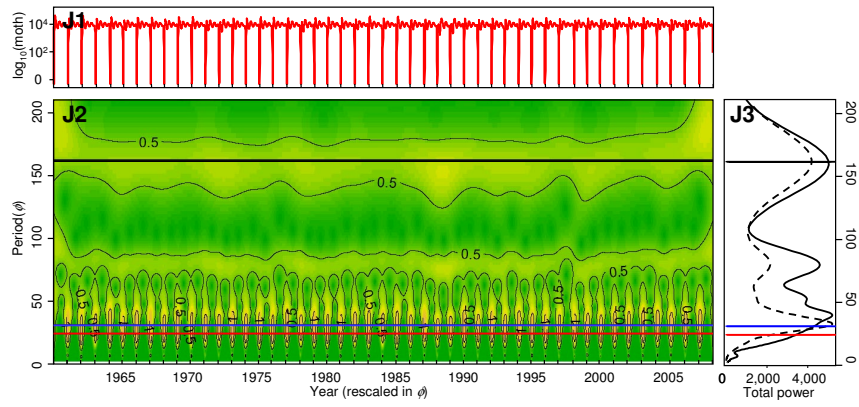


Fig. C10.— Illustrative model dynamics for Model J. See fig. C1 for legend details.

Model K

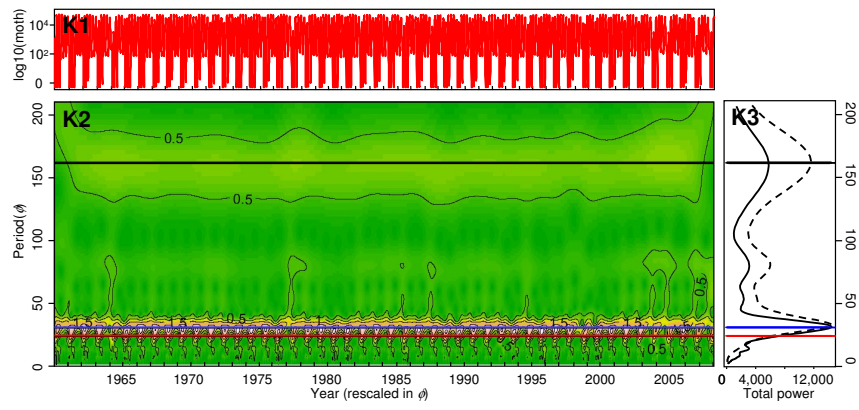


Fig. C11.— Illustrative model dynamics for Model K. See fig. C1 for legend details.

**Appendix D from T. Yamanaka et al., "Generation separation in simple structured life-cycles: models and 48 years of field data on a tea tortrix moth"**

**Model robustness to variation in stage development rates**

To assess the robustness of single-generation cycles in the fixed-delay model (online appendix B) to realistic variation in stage development rates, we develop a variant of the model with distributed stage durations. To construct the model, we assume that the delays in each stage are Gamma-distributed with an integer shape parameter, which is equivalent to dividing each stage into  $n$  substages, each with exponentially distributed substage duration. Following from online appendix B, the dynamics of each stage can be rewritten as

$$\frac{dC_{i,1}(\phi)}{d\phi} = n\alpha_{i-1}C_{i-1,n}(\phi) - n\alpha_i C_{i,1}(\phi) - \frac{\delta_i(\phi)}{m(\phi)}C_{i,1}(\phi) \quad (\text{D1})$$

$$\frac{dC_{i,j}(\phi)}{d\phi} = n\alpha_i (C_{i,j-1}(\phi) - C_{i,j}(\phi)) - \frac{\delta_i(\phi)}{m(\phi)}C_{i,j}(\phi) \quad (\text{D2})$$

where  $C_{i,j}$  is the density of individuals in substage  $j$  of stage  $i$ . If  $i = 1$ , then  $n\alpha_{i-1}C_{i-1,n}(\phi)$  is the birth rate  $\beta(\phi)/m(\phi)$ . Nabeta et al. (2005) report the standard error ( $SE$ ) and sample size  $x$  for the egg, larvae and pupae stage durations. We convert these numbers to estimates of standard deviations on the time-scale using  $\sigma = SE\sqrt{x}$ . The egg stage had a higher variance ( $\sigma_E^2 = 3.2$ ) than the larvae ( $\sigma_L^2 = 1.0$ ) or pupae stage ( $\sigma_P^2 = 0.6$ ). However, the influence of development rate variation on single-generation cycles in the model was not symmetric. We found that variance in the larvae, pupae and adult development rates had a large impact on the presence of limit cycles, but variance in the egg stage had no influence, so the remaining analyses are based on the variance in the larvae and pupae stages only. To compare the observed variation with the variation in the distributed delay model, we transformed the observed variance from the time-scale to the phi-scale using  $\sigma^2(\phi) = \sigma^2(t)(g(t)^2)$ , and calculate the scale ( $\kappa$ ) and shape ( $\theta$ ) parameters of a Gamma distribution using the expected larval stage duration using the data

of 20 °C from online appendix A and the variance ( $\kappa = 0.055$ ,  $\theta = 247.3$ ). The empirical distribution of stage durations corresponds to the distribution of stage durations predicted by the distributed delay model with roughly 200 substages (fig. D1), which has the same single-generation cycles as the fixed-delay model.

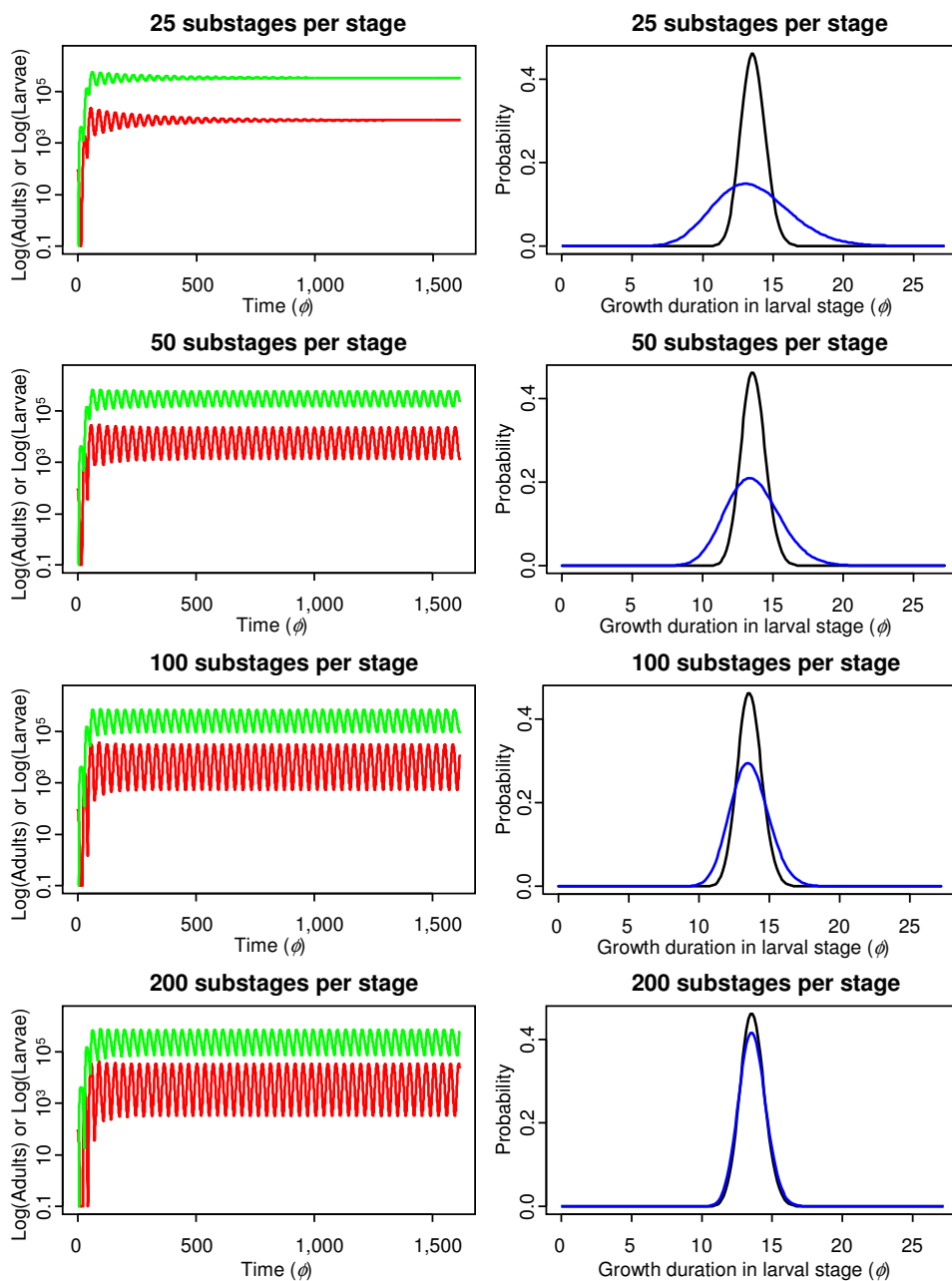


Fig. D1.— Influence of development rate variation on single-generation cycles. The left panels show population dynamics of larvae (green lines) and adult (red lines) of the model with adult senescence and without winter hardiness (corresponding to fig. 3). Right panels show the variation in the growth duration of the larval stage. Results are shown for  $n = 25, 50, 100,$  and  $200$  (blue lines). Observed variation in stage durations (dotted lines) corresponds to a distributed delay model with 200 substages per stage, which has the same dynamics as the fixed-delay model.